

Gamow-Teller transitions of neutron-rich $N = 82, 81$ nuclei by shell-model calculations

Noritaka Shimizu^{1,*}, Tomoaki Togashi¹, and Yutaka Utsuno^{2,1}

¹*Center for Nuclear Study, The University of Tokyo,*

7-3-1 Hongo, Bunkyo-ku, Tokyo 113-0033, Japan and

²*Advanced Science Research Center, Japan Atomic Energy Agency, Tokai, Ibaraki 319-1195, Japan*

β -decay half-lives of neutron-rich nuclei around $N = 82$ are key data to understand the r -process nucleosynthesis. We performed large-scale shell-model calculations in this region using a newly constructed shell-model Hamiltonian, and successfully described the low-lying spectra and half-lives of neutron-rich $N = 82$ and $N = 81$ isotones with $Z = 42 - 49$ in a unified way. We found that their Gamow-Teller strength distributions have a peak in the low-excitation energies, which significantly contributes to the half-lives. This peak, dominated by $\nu 0g_{7/2} \rightarrow \pi 0g_{9/2}$ transitions, is enhanced on the proton deficient side because the Pauli-blocking effect caused by occupying the valence proton $0g_{9/2}$ orbit is weakened.

I. INTRODUCTION

The solar system abundances and their peak structures indicate that major origin of most elements heavier than iron is generated by the r -process nucleosynthesis [1]. A neutron-star merger was found by measuring the gravitational wave which is followed by optical emission, called “kilonova” [2]. The properties of neutron-rich nuclei are key issues to reveal the r -process nucleosynthesis which is expected to occur in kilonova phenomena.

The r -process path is considered to go through the neutron-rich region of the nuclear chart. In the region where the r -process path comes across the magic number $N = 82$, these nuclei form the waiting points of neutron captures in the r -process. The path comes along the $N = 82$ line in the chart bringing about the so-called second peak of the natural abundance formed by the astrophysical r -process nucleosynthesis. In a typical r -process model, after reaching the ^{120}Sr ($Z = 38$, $N = 82$), the β -decay and the neutron capture are repeated alternately to generate $N = 82$ and $N = 81$ nuclei up to ^{128}Pd ($Z = 46$, $N = 82$) [3]. This repeated process occurs if the β -decay rates of $N = 81$ are smaller than their neutron-capture rates. Thus, the β -decay properties not only of the $N = 82$ isotones but also of the $N = 81$ ones are necessary to determine the r -process path, hence motivating the study of those very neutron-rich nuclei from the viewpoint of nuclear structure physics. Note that the properties of nuclei near $N = 82$ are also awaited in the context of fission recycling [4].

On the experimental side, β -decay half-lives of neutrino-rich nuclei around $N = 82$ have recently been measured by the EURICA campaign conducted at the RI Beam Factory in RIKEN Nishina Center [5, 6]. More detailed data are now available for some nuclei. Many isomers have been identified near the $N = 82$ shell gap, and some of their half-lives are obtained [7–10]. Furthermore, β -delayed neutron-emission probabilities and low-lying level structure have been measured [11, 12]. These data provide a stringent test for nuclear-structure models. It should be noted that similar experimental activities are extended to the $N = 126$ region, known as the third peak of the solar system abundance, for instance by the KISS (KEK Isotope Separator System) project [13].

Many theoretical efforts have also been paid to systematically calculate β -decay half-lives such as by FRDM [14], FRDM-QRPA [15], HFB-QRPA [16], DFT-QRPA [17, 18], and the gross theory [19]. Recently, further sophisticated methods were introduced into the systematic β -decay studies by introducing the FAM-QRPA [20] and by the relativistic CDFT-QRPA [21]. Novel machine-learning techniques were also applied to predict β -decay half-lives [22]. The nuclear shell-model calculation is also one of the most powerful theoretical schemes for this purpose. The previous shell-model studies are, however, restricted to calculating the half-lives of the singly-magic $N = 82$ [23–25] and $N = 126$ isotones [23, 26] due to the exponentially increasing dimensions of the Hamiltonian matrices in open-shell nuclei. The present work aims to extend those previous shell-model efforts to $N = 81$ isotones within a unified description of the structures of neutron-rich $N = 82$ and $N = 81$ isotones. The measured half-lives are well reproduced by the calculation, and we predict those for $^{125,126}\text{Ru}$, $^{124,125}\text{Tc}$ and ^{124}Mo . It is also predicted that these nuclei have rather strong GT strengths in the low excitation energies due to the increasing number of proton holes in the $g_{9/2}$ orbit, accelerating GT decay. This paper is organized as follows. The shell-model model space and its interaction are defined in Sect. II. Section III is devoted to the separation energies and low-lying spectra. The Gamow-Teller strength distribution and the half-lives are discussed in Sect. IV. Section V is devoted to the discussion of the enhancement of the GT transitions towards the proton-deficient nuclei and of its origin. This paper is summarized in Sect. VI.

II. FRAMEWORK OF SHELL-MODEL CALCULATIONS

We performed large-scale shell-model calculations of $N = 81$ and $N = 82$ isotones. The model space for the calculations is taken as $0f_{5/2}$, $1p_{3/2}$, $1p_{1/2}$, $0g_{9/2}$, $0g_{7/2}$, $1d_{5/2}$, $1d_{3/2}$, $2s_{1/2}$, and $0h_{11/2}$ for the proton orbits and $0g_{7/2}$, $1d_{5/2}$, $1d_{3/2}$, $2s_{1/2}$, and $0h_{11/2}$ for the neutrons orbits with the ^{78}Ni inert core. These orbits are shown in Fig. 1. Although we focus on $Z \leq 50$ nuclei in this study, the single-particle orbits beyond the $Z = 50$ shell gap are required to be included in the model space explicitly so that the Gamow-Teller transition causes the single-particle transition of the valence neutrons beyond $N = 50$ to the same orbits and its spin-orbit partners. The model space is extended from that of the earlier shell-model study [23] by adding the proton $0f_{5/2}$, $1p_{3/2}$, and $0h_{11/2}$ orbits. In the preceding shell-model works [23, 24], the proton $0h_{11/2}$ orbit was omitted to avoid the contamination of the spurious center-of-mass excitation, although the neutron occupying $0h_{11/2}$ orbit can decay to the proton occupied in $0h_{11/2}$ by the Gamow-Teller transition. In the present work, we explicitly include the proton $0h_{11/2}$ orbits into the model space so that the proton single-particle orbits cover the whole neutron orbits. For fully satisfying the Gamow-Teller sum rule the proton $0h_{9/2}$ orbit is required, but its single-particle energy is too high to significantly affect the Gamow-Teller strength of the low-lying states and it is omitted in the present work. The contamination of spurious center-of-mass excitation is removed by the Lawson method [27] with $\beta_{CM}\hbar\omega/A = 10$ MeV. We truncate the model space by restricting up to 2 proton holes in pf shell and up to 3 protons occupying the orbitals beyond the $Z = 50$ gap so that the numerical calculation is feasible. Even if applying such a truncation the M -scheme dimension of the shell-model Hamiltonian matrix reaches 3.1×10^9 and is quite large, and efficient usage of a supercomputer is essential. The shell-model calculations were mainly performed on CX400 supercomputer at Nagoya University and Oakforest-PACS at The University of Tokyo and University of Tsukuba utilizing the KSHELL shell-model code [28], which has been developed for massively parallel computation.

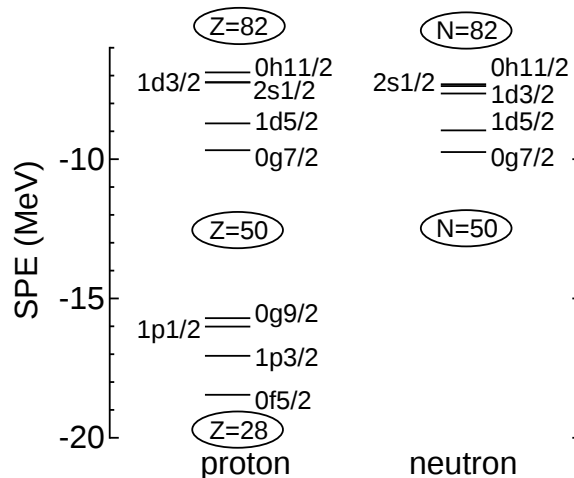


FIG. 1: Single-particle energies for ^{132}Sn determined from the experimental energy levels of its one-particle and one-hole neighboring nuclei [29–34]. The single-particle orbits taken as the model space are shown.

The effective realistic interaction for the shell-model calculation is constructed mainly by combining the two established realistic interactions: the JUN45 interaction [35] for the f_5pg_9 model space and the SNBG3 interaction [36] for the neutron model space of $50 < N, Z < 82$. The JUN45 and SNBG3 interactions were constructed from the G-matrix interaction with phenomenological corrections using a chi-square fit to reproduce experimental energies. For the rest part of the two-body matrix elements (TBMEs), we adopt the monopole-based universal (V_{MU}) interaction [37] whose $T = 1$ central force is scaled by the factor 0.75 in the same way as Ref. [38]. The single particle energies are determined to reproduce the experimental energies of one-nucleon neighboring nuclei of ^{132}Sn as shown in Fig. 1. In addition, the strengths of the pairing interaction and the diagonal TBMEs of the $(\pi 0g_{9/2}, \pi 0g_{9/2})$ and $(\pi 0g_{9/2}, \nu 0h_{11/2})$ orbits are modified to reproduce the experimental energy levels of ^{130}Cd , ^{128}Pd , and ^{130}In . The TBMEs are assumed to have the mass dependence $(A/132)^{-0.3}$.

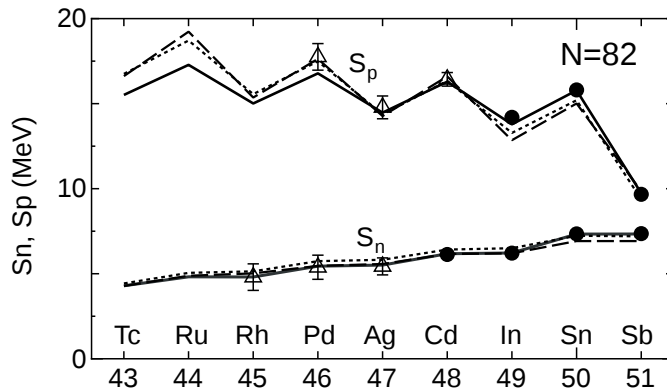


FIG. 2: Separation energies of $N = 82$ isotones. The solid lines show the proton and neutron separation energies provided by the present shell-model study. The filled circles and the open triangles with error bars denote the experimental values and the extrapolated values from the experimental systematics, respectively [39]. The dotted lines and the dashed lines are given by the KTUY mass formula [40] and the FRDM [14].

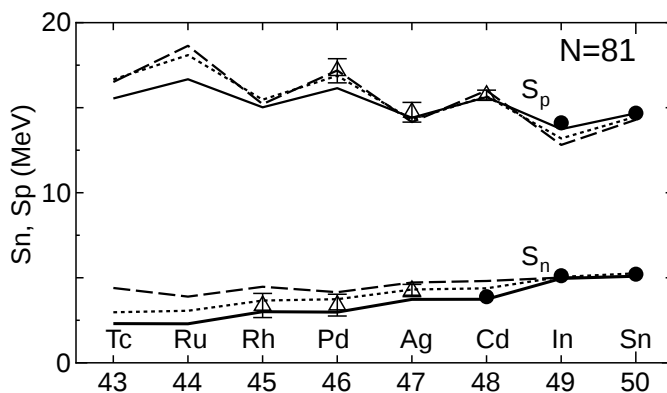


FIG. 3: Separation energies of $N = 81$ isotones. See the caption of Fig. 2 for details.

III. SEPARATION ENERGIES AND EXCITATION ENERGIES

The binding energies and excitation energies of the $N = 82$ nuclei and those around them are important not only for describing the β -decay properties, but also for confirming the validity of the shell-model interaction. Figures 2 and 3 show the proton and neutron separation energies of the $N = 82$ and $N = 81$ isotones, respectively. The present shell-model results reproduce the experimental values excellently. The neutron separation energy determines the threshold energy of the β -delayed neutron emission, which is important for the r -process nucleosynthesis. Since the Q -value of the β^- decay is obtained using the proton and neutron separation energies as

$$\begin{aligned} Q(\beta^-, Z, N) &= BE(Z+1, N-1) - BE(Z, N) + (m_n - m_p - m_e)c^2 \\ &= S_p(Z+1, N) - S_n(Z+1, N) + 0.782 \text{ MeV}, \end{aligned} \quad (1)$$

where $BE(Z, N)$ denotes the binding energy of the (Z, N) nucleus and 0.782 MeV is obtained from the mass difference of a neutron, a proton and an electron. The Q values of β -decay given by the shell-model results are in good agreement with the available experimental values, as shown as the difference of S_n and S_p in Figs. 2 and 3. For comparison, the result of the KTUY [40] and the FRDM [14] mass formulae are also plotted in the figures, showing very good agreement with the experimental values except slight underestimation in the proton separation energy of ^{130}In . On the proton deficient side where the experimental values are not available, the difference among the theoretical predictions gradually increases as the proton number decreases, while the neutron separation energies of the $N = 82$ isotones are rather close to one another.

Figure 4 shows low-lying energy levels in the neutron-rich $N = 82$ isotones from $Z = 42$ to $Z = 50$. For the nuclei without data, we plot a few lowest levels obtained by the calculation. The calculated ground states are 0^+ for the even- Z isotopes and $9/2^+$ for the odd- Z isotopes. The experimental levels are reproduced excellently by the shell-model results. The levels of ^{129}Ag are experimentally unknown, but two β -decaying states were found and tentatively

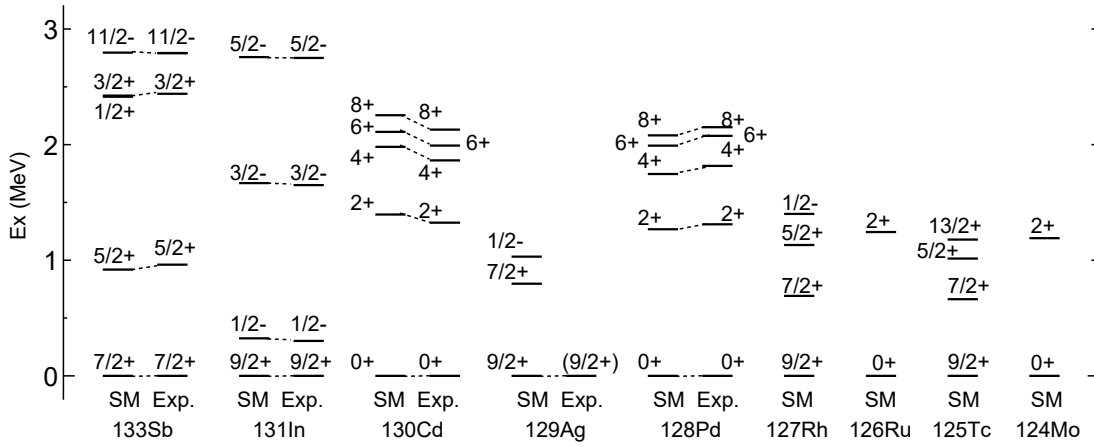


FIG. 4: Excitation energies of $N = 82$ isotones: ^{133}Sb , ^{131}In , ^{130}Cd , ^{129}Ag , ^{128}Pd , ^{127}Rh , ^{126}Ru , ^{125}Tc , and ^{124}Mo compared between the shell model (SM) and experiment (Exp.) [34].

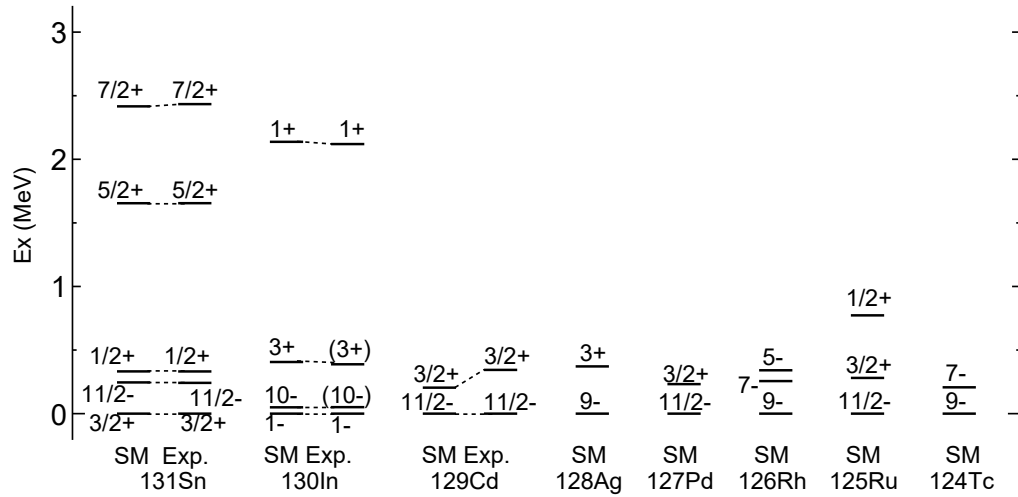


FIG. 5: Excitation energies of $N = 81$ isotones: ^{131}Sn , ^{130}In , and ^{129}Cd , ^{128}Ag , ^{127}Pd , ^{126}Rh , ^{125}Ru , and ^{124}Tc . See the caption of Fig. 4 for details.

assigned as $9/2^+$ and $1/2^-$ [34] without their excitation energies known. In the present calculation, the $1/2^-$ state is located very close to the $7/2^+$ state. Considering a long $E3$ half-life in such a case, it is reasonable to assume that the $1/2^-$ state predominantly decays through β emission.

Figure 5 shows the excitation spectra of the $N = 81$ isotones. Unlike the $N = 82$ isotones, several candidates for the ground state and some β -decaying isomers are predicted. This is partly because the $1d_{3/2}$ and the $0h_{11/2}$ neutron orbits are located very close in energy as known in the spectra of ^{131}Sn and the difference of their spin numbers is large. For ^{129}Cd , two β -decaying states with $11/2^-$ and $3/2^+$ were known and their order had been controversial [7]. A recent experiment concluded that its ground-state spin is $11/2^-$ and the excitation energy of $3/2^+$ is $343(8)$ keV [10, 11], which is consistent with our shell-model prediction. For ^{127}Pd , no experimental energy levels are known, and the present order of $11/2^-$ and $3/2^+$ agrees with another shell-model prediction [45]. With regard to β -decay properties, the excitation energy of the 1^+ state of ^{130}In plays a crucial role in the β -decay half-life of ^{130}Cd [24], whose 0^+ ground state decays to the lowest 1^+ state most strongly with the Gamow-Teller transition.

Figure 6 shows the calculated energy levels of the $N = 80$ and $N = 79$ isotones for which the experimental data are available. We confirm a reasonable agreement between them.

The present calculation reproduces the experimental energies quite well, thus confirming the validity of the model space and the effective interaction employed in the present shell-model calculation.

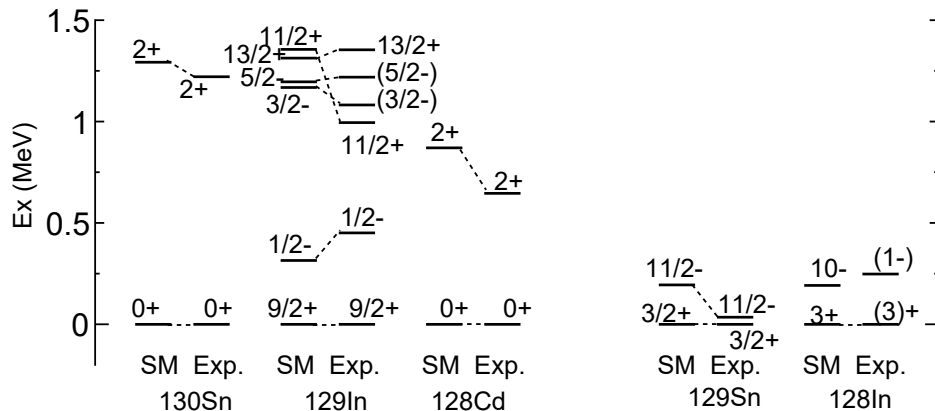


FIG. 6: Excitation energies of the $N = 80$ isotones (^{130}Sn , ^{129}In , and ^{128}Cd) and the $N = 79$ isotones (^{129}Sn and ^{128}In). The experimental values are taken from Refs. [11, 34]. See the caption of Fig. 4 for details.

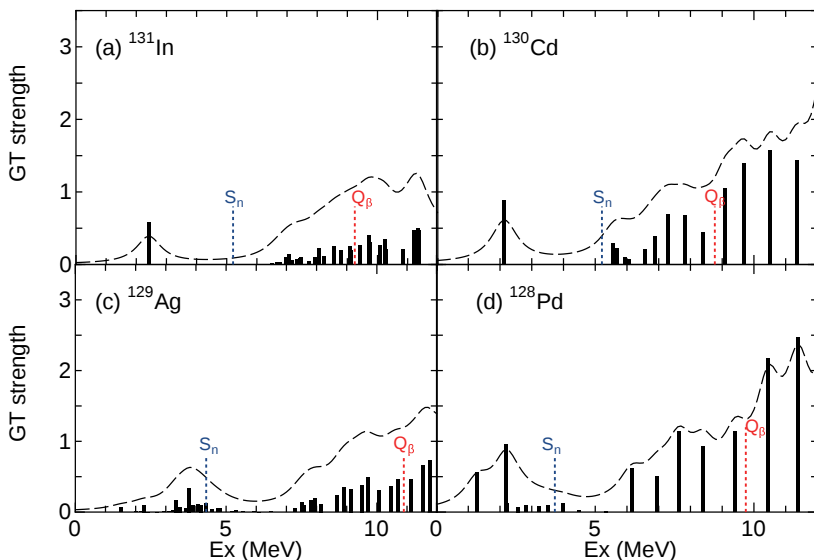


FIG. 7: Gamow-Teller strength functions of $N = 82$ isotones, (a) ^{131}In , (b) ^{130}Cd , (c) ^{129}Ag , and (d) ^{128}Pd against the excitation energies of the daughter nuclei. The dashed lines are the folded strength functions by a Lorentzian function with the 1-MeV width. The values are shown without the quenching factor. The Q_β values and the neutron separation energies are shown as the red dotted lines and the blue dotted lines, respectively.

IV. GAMOW-TELLER STRENGTH FUNCTION AND β^- -DECAY HALF-LIVES

We calculated the Gamow-Teller β^- -strength functions for $N = 82$ and $N = 81$ neutron-rich nuclei to estimate their half-lives. We adopted the Lanczos strength function method [41–43] with 250 Lanczos iterations to obtain sufficiently converged results. The magnitude of quenching of axial vector coupling is still a challenging topic for nuclear physics and has large uncertainty mainly caused by nuclear medium effect and many-body correlations. In the present work, the quenching factor is taken as $q_{\text{GT}} = 0.7$, which has been most widely used [26, 44] and is consistent with the adopted value of the preceding work, $q_{\text{GT}} = 0.71$ [24]. The first-forbidden transition is omitted in the present work because its contribution to the half-lives is small, around 13%, and rather independent of nuclides for the $Z = 42 - 48$, $N = 82$ isotones in a previous shell-model study [23]. Furthermore, it is pointed out in [11] that a number of allowed transitions are observed in the β^- decays of $^{121-131}\text{In}$ and $^{121-125}\text{Cd}$, suggesting the dominance of GT transitions in the low excitation energies. This point will be discussed later.

Figure 7 shows the Gamow-Teller distributions of $N = 82$ isotones, ^{131}In ($Z = 49$), ^{130}Cd ($Z = 48$), ^{129}Ag ($Z = 47$), and ^{128}Pd ($Z = 46$). Figure 8 shows those of more proton-deficient $N = 82$ isotones, ^{127}Rh ($Z = 45$), ^{126}Ru ($Z = 44$), ^{125}Tc ($Z = 43$), and ^{124}Mo ($Z = 42$). The Q -values are taken from the experiments for ^{131}In and ^{130}Cd [34], while the present theoretical Q -values are used for the other nuclei. These figures present a very remarkable systematics of low-

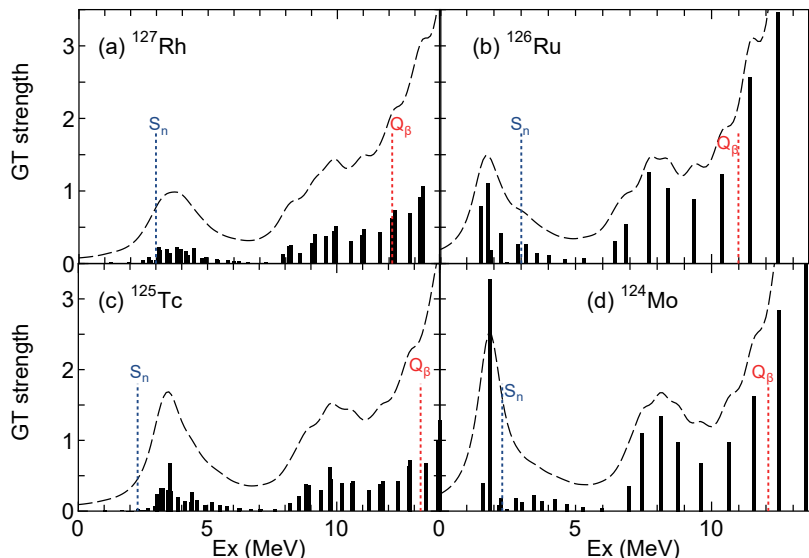


FIG. 8: Gamow-Teller strength functions of proton-deficient $N = 82$ isotones, (a) ^{127}Rh , (b) ^{126}Ru , (c) ^{125}Tc , and (d) ^{124}Mo . See the caption of Fig. 7 for details.

$T_{1/2}(\text{ms}), N = 82$	SM th	SM ^{exp}	SM13	SM07	SM99	Exp15	Exp16
$^{131}\text{In} \rightarrow ^{131}\text{Sn}$	156	154	247.53	260	177	261(3)	265(8)
$^{130}\text{Cd} \rightarrow ^{130}\text{In}$	158	116	164.29	162	146	127(2)	126(4)
$^{129}\text{Ag} \rightarrow ^{129}\text{Cd}$	44		69.81	70	35.1	52(4)	
$^{128}\text{Pd} \rightarrow ^{128}\text{Ag}$	28		47.25	46	27.3	35(3)	
$^{127}\text{Rh} \rightarrow ^{127}\text{Pd}$	13.9		27.98	27.65	11.8	20_{-7}^{+20}	
$^{126}\text{Ru} \rightarrow ^{126}\text{Rh}$	9.2		20.33	19.76	9.6		
$^{125}\text{Tc} \rightarrow ^{125}\text{Ru}$	5.7		9.52	9.44	4.3		
$^{124}\text{Mo} \rightarrow ^{124}\text{Tc}$	4.0		6.21	6.13	3.5		

TABLE I: β -decay half-lives of the $N = 82$ isotones by the present shell-model calculations (SM), the shell-model study with the experimental Q value (SM^{exp}), the earlier shell-model works (SM13 [23]), (SM07 [24]), (SM99 [25]), and the recent experiments (Exp15) [6], (Exp16) [7]. The half-lives are shown in the unit of ms.

energy GT strength distributions, which play a crucial role in those β -decay half-lives. First, all the $N = 82$ isotones considered here have strong GT strengths in the low-excitation energies. Except ^{131}In , they are peaked at ~ 3.5 MeV and ~ 2 MeV for the odd- Z and even- Z parents, respectively, and the GT strengths are more concentrated for the even- Z isotopes. This odd-even effect is in accordance with what is found in the sd - pf shell region [48]. Second, this low-energy GT peak grows with decreasing proton number. This is an interesting feature of low-energy Gamow-Teller transitions predicted for this region, and more detailed discussions will be given in Sec. V.

Table I shows the β -decay half-lives of the $N = 82$ isotones. The half-life is estimated by accumulating the transition probabilities from the parent ground state to the daughter states whose excitation energies are below the Q_β value. The shell-model results show reasonable agreement with the experimental values. While the present half-lives of ^{129}Ag and ^{128}Pd are closer to the experimental values than the earlier shell-model result, the half-life of ^{131}In is underestimated. This underestimation is caused by the large GT transition to the lowest $7/2^+$ state of the daughter ^{131}Sn at $E_x = 2.4$ MeV, which might imply the need for further improvement of the theoretical model. This state is considered to be dominated by the $\nu 0g_{7/2}$ -hole state of ^{132}Sn . In the pure $\pi 0g_{9/2}^{-1} \rightarrow \nu 0g_{7/2}^{-1}$ single-particle transition, the corresponding $B(\text{GT})$ value is as much as 1.78 without the quenching factor introduced. On the other hand, the present calculation gives $B(\text{GT}) = 0.58$. This value is considerably reduced from the single-particle value due to configuration mixing, but further reduction is required to completely reproduce the data.

For comparison, Table I also shows three shell-model results by the Strasbourg group: SM13 [23], SM07 [24], and SM99 [25]. The half-lives of ^{126}Ru , ^{125}Tc , and ^{124}Mo predicted by the present calculation are close to those of SM99 [25]. The half-lives of SM13 [23] and SM07 [24] are quite close to each other. While the first-forbidden transition was omitted and the quenching factor of the Gamow-Teller transition was taken as $q_{\text{GT}} = 0.71$ in SM07, the first-forbidden transition is included with $q_{\text{GT}} = 0.66$ in SM13. The agreement of these results indicates that the contribution of the first-forbidden decay is rather independent of the nuclides and can be absorbed into the minor change of the

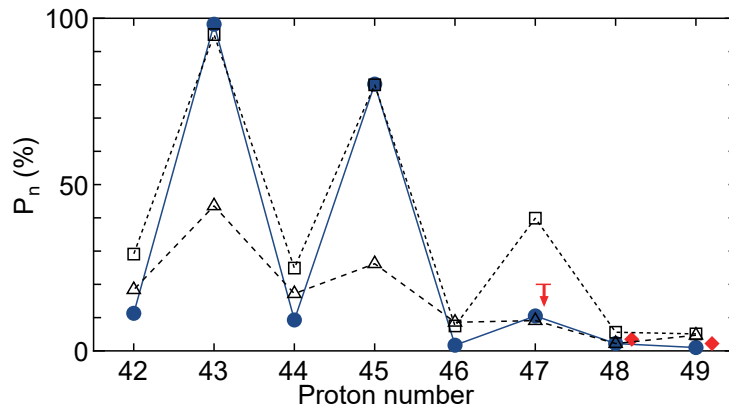


FIG. 9: Neutron emission probabilities of $N = 82$ isotones. The blue filled circles, black open squares, and black open triangles denote the results by the present work, the earlier shell-model work [23], and the FRDM+QRPA [15], respectively. The red diamond denotes the experimental value and the red line with an arrow at $Z = 47$ denotes the experimental upper limit [46, 47].

$T_{1/2}(\text{ms}), N = 81$	SM th	SM ^{exp}	Exp15	Exp16
$^{130}\text{In} \rightarrow ^{130}\text{Sn}$	286	311	284(10)	
$^{129}\text{Cd} \rightarrow ^{129}\text{In}$	182	139	154.5(20)	147(3)
$^{129}\text{Cd} (3/2^+) \rightarrow ^{129}\text{In}$	266	181		157(8)
$^{128}\text{Ag} \rightarrow ^{128}\text{Cd}$	49		59(5)	
$^{127}\text{Pd} \rightarrow ^{127}\text{Ag}$	32		38(2)	
$^{126}\text{Rh} \rightarrow ^{126}\text{Pd}$	17		19(3)	
$^{125}\text{Ru} \rightarrow ^{125}\text{Rh}$	11			
$^{124}\text{Tc} \rightarrow ^{124}\text{Ru}$	7.0			

TABLE II: β -decay half-lives of the $N = 81$ isotones obtained by the present shell-model study (SMth), the shell-model study with the experimental Q value (SM^{exp}), and the experiments (Exp15) [6], (Exp16) [7]. The half-lives are shown in the unit of ms. The half-life of the $3/2^+$ isomeric state of ^{129}Cd is also shown.

Gamow-Teller quenching factor in this mass region.

β -delayed neutron emission is important for understanding the freezeout of the r process [1]. Figure 9 show β -delayed neutron emission probabilities P_n for $N = 82$ nuclei. In the present calculation, we accumulate the probabilities of the β -decay to the states above the neutron-emission threshold S_n to obtain P_n . The present shell-model results show an odd-even staggering similar to that of the earlier shell model [23], while the FRDM-QRPA results show weaker odd-even staggering. This odd-even staggering is caused by the difference of the peak position and the degree of concentration of the Gamow-Teller transition strengths. As discussed already using Figs. 7 and 8, the GT peaks of the even- Z parent nuclei are located at around $E_x = 2$ MeV, which is lower than S_n , causing their small P_n values. For ^{124}Mo , it is predicted that this low-energy GT strength is concentrated by a single peak that is located slightly below S_n . Hence its P_n is very sensitive to the detail of the energies concerned. For the odd- Z nuclei of ^{127}Rh and ^{125}Tc , the low-energy GT peak is located higher than S_n , enlarging their P_n values.

Figures 10 and 11 show the Gamow-Teller β^- -strength distribution of $N = 81$ isotones, namely ^{130}In , ^{129}Cd , ^{128}Ag , ^{127}Pd , ^{126}Rh , ^{125}Ru and ^{124}Tc obtained by the present shell-model calculations. Figures 11 shows also the distribution of the isomeric $3/2^+$ state of ^{129}Cd . The $Q(\beta^-)$ values are taken from experiments for ^{130}In and ^{129}Cd [34], and taken from shell-model values for the other nuclei. The low-energy GT peaks are obtained in all the cases calculated. They are located higher for the odd- Z parents due to pairing correlation in the daughter nuclei, but fragmented in a similar manner. Like the case of the $N = 82$ isotones, those peaks are enhanced as the proton number decreases and the proton $0g_{9/2}$ orbit becomes unoccupied.

Table II shows the β -decay half-lives of the $N = 81$ isotones. The half-lives of the five nuclei with $Z \geq 45$ show reasonable agreement with the available experimental values, indicating the validity of the present shell-model calculation. The half-life of the $3/2^+$ isomeric state of ^{129}Cd is also shown in the table to demonstrate the capability to obtain the β -decay rates of isomeric states.

In Tables I and II, SMth and SM^{exp} show the shell-model results using the shell-model Q value and those using the experimental Q value, respectively, to discuss the uncertainty of the present theoretical model. The deviations of the choice of the Q values show up to 30% at most. The fitted quenching factor to reproduce the experimentally measured half-lives of ^{129}Cd , ^{130}Cd and the $3/2^+$ isomer by the SM^{exp} result is $q_{\text{GT}} = 0.67$, which shows a 9% increase of the

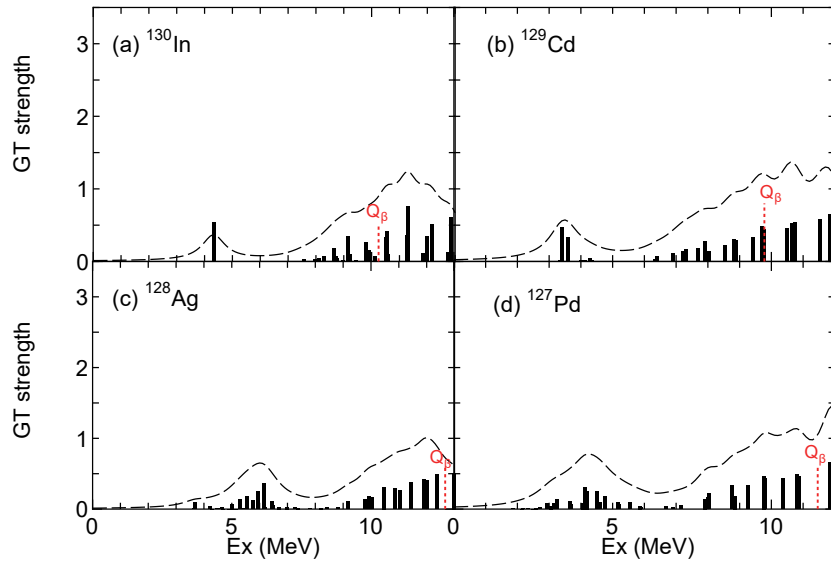


FIG. 10: Gamow-Teller strength functions of $N = 81$ isotones, (a) ^{130}In , (b) ^{129}Cd , (c) ^{128}Ag , and (d) ^{127}Pd . See the caption of Fig. 7 for details.

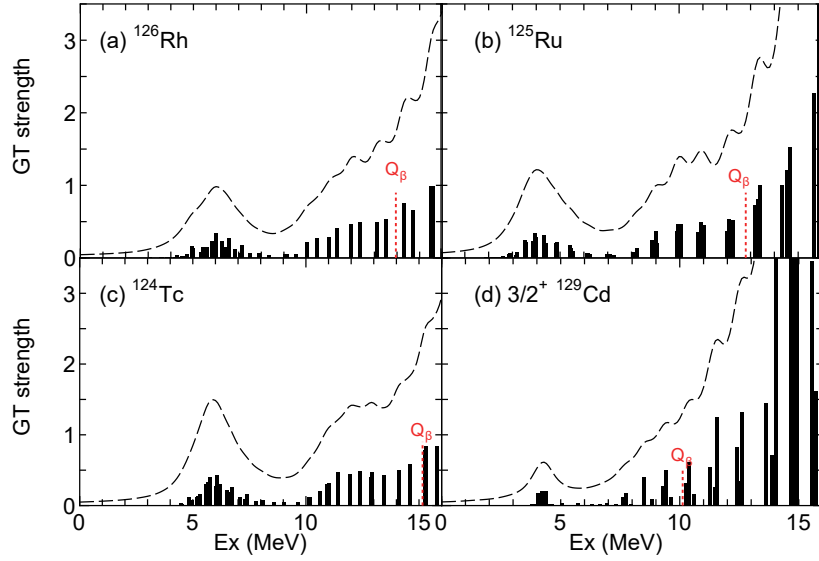


FIG. 11: Gamow-Teller strength functions of $N = 81$ isotones, (a) ^{126}Rh , (b) ^{125}Ru , (c) ^{124}Tc , and (d) the isomeric $3/2^+$ state of ^{129}Cd . See the caption of Fig. 7 for details.

half-life estimate. These differences are considered as the uncertainties of the present model.

V. POSSIBLE OCCURRENCE OF SUPERALLOWED GAMOW-TELLER TRANSITIONS TOWARD $Z = 40$

As mentioned in the last section, Figures 7 and 8 show that for the even- Z parents a low-energy Gamow-Teller peak emerges at ~ 2 MeV and that its magnitude is enhanced as the proton number decreases. As depicted in Fig. 12, this peak is finally concentrated in a single state at ^{122}Zr with $Z = 40$, leading to $B(\text{GT}) = 2.7$ calculated with the quenching factor 0.7. In this section, we focus on this growing Gamow-Teller peak toward $Z = 40$.

At first, we discuss why this peak is enlarged with decreasing Z . By analyzing one-body transition densities obtained in the present calculations, one can see that those low-energy Gamow-Teller peaks are dominated by the $\nu 0g_{7/2} \rightarrow \pi 0g_{9/2}$ transition. If the $\pi 0g_{9/2}$ orbit is completely filled, this transition does not occur due to the Pauli

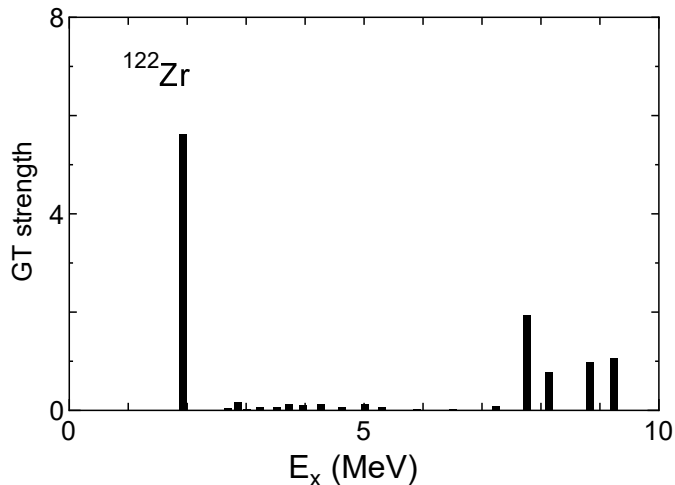


FIG. 12: Gamow-Teller strength functions of ^{122}Zr . See the caption of Fig. 7 for details.

blocking. This blocking effect is weakened by removing protons from the $\pi 0g_{9/2}$ orbit, hence the enlargement of the low-energy Gamow-Teller peak.

The resulting $B(\text{GT})$ values of this peak are particularly large at ^{124}Mo and ^{122}Zr compared to typical values. It is known from the systematics [49] that the $\log ft$ values of allowed β decays are distributed around $\log ft \sim 6$, which corresponds to $B(\text{GT}) \sim 10^{-3}$ - 10^{-2} for Gamow-Teller transitions. A well-known deviation from this systematics is the superallowed (Fermi) transition. When isospin is a good quantum number, the Fermi transition occurs only between isobaric analog states, giving a typical $\log ft$ of 3.5. With regard to Gamow-Teller transitions, however, there are only a few cases where the $\log ft$ value is comparable to those of the superallowed Fermi transitions because of the fragmentation of Gamow-Teller strengths. Since $B(\text{GT}) = 1$ leads to $\log ft = 3.58$, the $B(\text{GT})$ value of the order of unity is a good criterion to compare the superallowed Fermi transition.

It is proposed in [50] that such extraordinarily fast Gamow-Teller transitions be classified as Super Gamow-Teller transitions. At that time, only two Gamow-Teller transitions, $^6\text{He} \rightarrow ^6\text{Li}$ and $^{18}\text{Ne} \rightarrow ^{18}\text{F}$, were known to satisfy the condition of Super Gamow-Teller transition defined in [50], i.e., $B(\text{GT}) > 3$. These large Gamow-Teller strengths are caused by the constructive interference of $j_> \rightarrow j_>$ and $j_> \rightarrow j_<$ matrix elements [51]. It was also predicted in [50] that two $N = Z$ doubly-magic nuclei ^{56}Ni and ^{100}Sn were candidates for nuclei causing Super Gamow-Teller transitions. Although the Gamow-Teller strengths from ^{56}Ni were measured to be fragmented about a decade later [52], ^{100}Sn is now established to have a very large $B(\text{GT})$ value ($9.1_{-2.6}^{+3.0}$ in [53] or $4.4_{-0.7}^{+0.9}$ in [54]) to a 1^+ state located at around 3 MeV. This Gamow-Teller decay is called “superallowed Gamow-Teller” decay in [53] on the analogy of the superallowed Fermi decay.

The $B(\text{GT})$ values predicted for ^{124}Mo and ^{122}Zr in the present study are the order of unity, although not reaching the measured value of ^{100}Sn . Thus, they are new candidates for the superallowed Gamow-Teller transitions. Interestingly, those two regions of superallowed Gamow-Teller transition share the same underlying mechanism. In the extreme single-particle picture, the $\pi 0g_{9/2}$ orbit is completely filled and the $\nu 0g_{7/2}$ orbit is completely empty in ^{100}Sn . Since the former and the latter orbits are the highest occupied and the lowest unoccupied ones, respectively, its low-energy Gamow-Teller transition is caused by the $\pi 0g_{9/2} \rightarrow \nu 0g_{7/2}$ transition. On the other hand, in ^{122}Zr , the $\nu 0g_{7/2}$ orbit is completely filled and the $\pi 0g_{9/2}$ orbit is completely empty. As for the order of single-particle levels, Fig. 13 shows the evolution of the effective single-particle energies of $N = 82$ isotones as a function of Z . For protons, the $\pi 0g_{9/2}$ orbit keeps the lowest unoccupied orbit in this range. For neutrons, although the $\nu 0g_{7/2}$ orbit is the lowest at $Z = 50$ among the five orbits of interest, it goes up higher with decreasing Z to finally be the second highest at $Z = 40$. This is caused by a particularly strong attractive monopole interaction between $\pi 0g_{9/2}$ and $\nu 0g_{7/2}$ due to a cooperative attraction of the central and the tensor forces [37]. This sharp change of the $\nu 0g_{7/2}$ orbit in going from $Z = 40$ to 50 is established from the energy levels of ^{91}Zr and ^{101}Sn , as mentioned in [37]. In ^{122}Zr , the $\nu 0g_{7/2}$ orbit is thus close to the highest occupied level, making a low-energy Gamow-Teller state by the $\nu 0g_{7/2} \rightarrow \pi 0g_{9/2}$ transition. If one is restricted to the configuration most relevant to the low-energy Gamow-Teller transition, the final state of the ^{122}Zr decay, $(\nu 0g_{7/2})^{-1}(\pi 0g_{9/2})^{+1}$, is the particle-hole conjugation of that of the ^{100}Sn decay, $(\pi 0g_{9/2})^{-1}(\nu 0g_{7/2})^{+1}$. A schematic illustration of these configurations are given in Fig. 14. Accordingly, the $B(\text{GT})$ values from the vacuum to these single-particle configurations, i.e., those of Fig. 14(a) and (b), are identical.

One of the important ingredients for making $B(\text{GT})$ large in those nuclei is that the $B(\text{GT})$ value obtained within

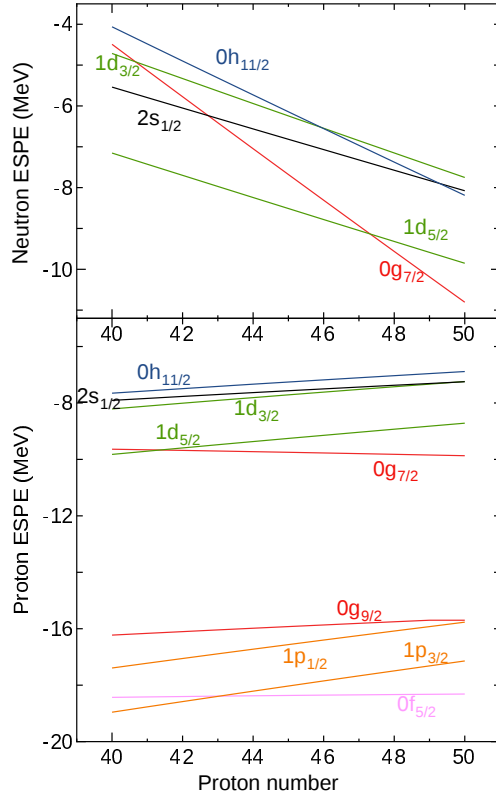


FIG. 13: Effective single-particle energies of the $N = 82$ isotones for neutron orbits (upper) and proton orbits (lower) as a function of the proton number calculated with the Hamiltonian used in this study.

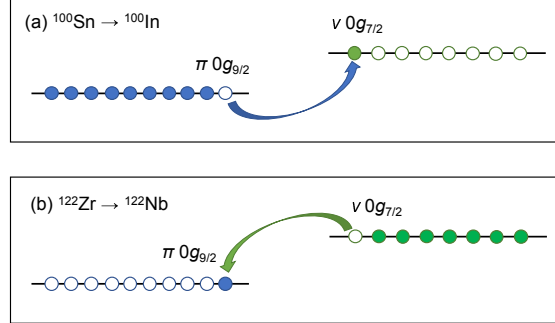


FIG. 14: Schematic illustration of the dominant single-particle transition in (a) the β^+ decay of ^{100}Sn and (b) the β^- decay of ^{122}Zr . The filled and open circles denote particles and holes, respectively.

the single configuration of Fig. 14 (a) [and (b)] is also large. To be more specific, let us compare two cases as the initial state, (i) $|(\pi 0g_{9/2})^{10}; J = 0\rangle$ and (ii) $|(\pi 0g_{9/2})^2; J = 0\rangle$, where one proton can move to the $\nu 0g_{7/2}$ orbit through the Gamow-Teller transition. The case (i) corresponds to Fig. 14(a) and yields $B(\text{GT})=17.78$ (without the quenching factor), whereas the case (ii) gives $B(\text{GT})=3.56$. The ratio of these two $B(\text{GT})$ values, 10 to 2, is just that of the number of protons in the initial state. This proportionality is well understood by remembering the Ikeda sum rule.

Although the $B(\text{GT})$ value in the extreme single-particle picture is as large as 17.78 for the configurations of Figs. 14 (a) and (b), it is reduced in reality by the quenching factor and fragmentation over other excited states. To minimize fragmentation, it is desirable to suppress the level density with the same J^π near the state of interest. ^{100}Sn and ^{122}Zr are doubly-magic (or semi-magic) nuclei, thus having a favorable condition for that. Another important factor to affect level density is excitation energy. As presented in Figs. 7, 11 and 12, the low-energy Gamow-Teller peak is located stably at around 2 MeV by changing Z . This excitation energy is low enough to isolate the peak, if one remembers that the superallowed Gamow-Teller state from the ^{100}Sn decay is located at ~ 3 MeV. In the present calculations, we do not include neutron excitations beyond the $N = 82$ shell gap. Since these excitations typically

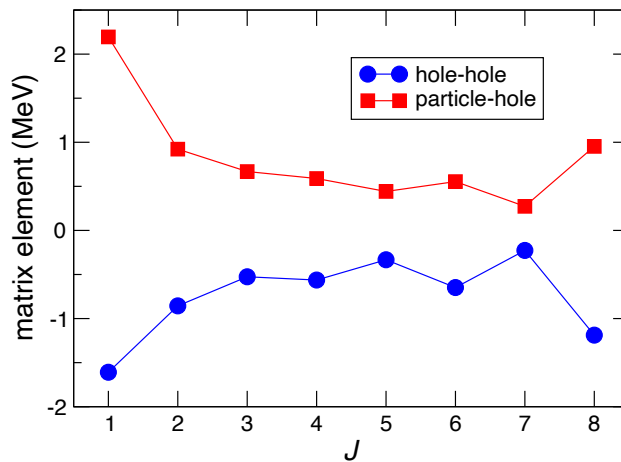


FIG. 15: Hamiltonian matrix elements concerning the $\pi 0g_{9/2}$ and $\nu 0g_{7/2}$ orbits used in this study. The circles and the squares are the hole-hole matrix elements, $\langle (\pi 0g_{9/2})^{-1} (\nu 0g_{7/2})^{-1} | V | (\pi 0g_{9/2})^{-1} (\nu 0g_{7/2})^{-1} \rangle_J$ and the particle-hole matrix elements, $\langle \pi 0g_{9/2} (\nu 0g_{7/2})^{-1} | V | \pi 0g_{9/2} (\nu 0g_{7/2})^{-1} \rangle_J$, respectively.

cost more than 4 MeV by estimating from the first excitation energy of ^{132}Sn , they probably do not contribute much to fragmentation.

One may wonder why the low-energy Gamow-Teller peak is kept at $E_x \sim 2$ MeV from $Z = 48$ to $Z = 40$ in spite of the sharp change of the $\nu 0g_{7/2}$ energy as shown in Fig. 13. This is due to the nature of two-body Hamiltonian matrix elements. The low-energy Gamow-Teller state has always a neutron hole in $0g_{7/2}$. For the nuclei close to $Z = 50$, this state has a few proton holes in $0g_{9/2}$, and thus its excitation energy is dominated by the hole-hole matrix element $\langle (\pi 0g_{9/2})^{-1} (\nu 0g_{7/2})^{-1} | V | (\pi 0g_{9/2})^{-1} (\nu 0g_{7/2})^{-1} \rangle_{J=1}$ as well as the single-particle energy of $\nu 0g_{7/2}$. As presented in Fig. 15, this matrix element is the most attractive among the possible J values. Hence the low-energy Gamow-Teller state is located lower than the simple estimate that the $0g_{7/2}$ orbit lies ~ 3 MeV below the Fermi surface at $Z = 50$ (see Fig. 13).

This situation changes as more protons are removed from the $\pi 0g_{9/2}$ orbit. For the nuclei close to $Z = 40$, the number of particles are smaller than the number of holes in the $0g_{9/2}$ orbit, and the particle-hole matrix element $\langle \pi 0g_{9/2} (\nu 0g_{7/2})^{-1} | V | \pi 0g_{9/2} (\nu 0g_{7/2})^{-1} \rangle_J$ plays a dominant role. In Fig. 15, we also show the particle-hole matrix elements that are derived from the hole-hole matrix elements by using the Pandya transformation. The $J = 1$ coupled matrix element has the largest positive value, thus losing the largest energy. This explains the calculated result that the low-energy Gamow-Teller state is not drastically lowered toward $Z = 40$ as expected from the evolution of the $\nu 0g_{7/2}$ orbit, and also the observation that the corresponding state for the ^{100}Sn decay is located at ~ 3 MeV [53]. It should be noted that this J dependence is an example of the parabolic rule that holds for short-range attractive forces [55].

To briefly summarize this section, the predicted superallowed Gamow-Teller transition toward $Z = 40$ occurs due to (a) the full occupation of a neutron high- j orbit ($\nu 0g_{7/2}$ in this case) and the emptiness of its proton spin-orbit partner ($\pi 0g_{9/2}$ in this case) and (b) the low excitation energy of the $J = 1$ particle-hole state created by these two orbits. Since the $J = 1$ proton-neutron particle-hole matrix elements are generally most repulsive among possible J , it is needed to fulfill (b) that the $\nu 0g_{7/2}$ orbit and the $\pi 0g_{9/2}$ orbit are closed to the highest occupied orbit and the lowest unoccupied orbit, respectively. The tensor-force driven shell evolution plays a crucial role in satisfying this condition.

VI. SUMMARY

We have constructed a shell-model effective interaction and performed large-scale shell-model calculations of neutron-rich $N = 82$ and $N = 81$ nuclei by utilizing our developed shell-model code and the state-of-the-art supercomputers. We demonstrated that the experimental binding and excitation energies of neutron-rich $N = 79, 80, 81$ nuclei are well reproduced by the available experimental data including the low-lying excited states. The present study gives the Gamow-Teller strength functions and the β -decay half-lives of $N = 82$ and $N = 81$ nuclei, which are reasonably consistent with the available experimental data, and several predictions for further proton-deficient nuclei. In these isotones, as the proton number decreases from $Z = 49$ to $Z = 42$, the proton $0g_{9/2}$ orbit becomes unoccupied

and the Gamow-Teller strengths of the low-lying states increases because of the Pauli-blocking effect. We predict that the low-energy Gamow-Teller strength is further enlarged in ^{122}Zr to make its $\log ft$ value equivalent to that of the superallowed beta decay. This is quite an analogous case to the so-called “superallowed Gamow-Teller” transition observed in ^{100}Sn in terms of Gamow-Teller strength and underlying mechanism.

In the present work, we assume the contribution of the first-forbidden transition is independent of the nuclides and can be absorbed into a single quenching factor of the Gamow-Teller transition. Further investigation to estimate the first-forbidden decay especially for the $N = 81$ isotones is also expected.

Acknowledgment

We acknowledge Takaharu Otsuka and Michio Honma for valuable discussions. A major part of shell-model calculations was performed on CX400 supercomputer of Nagoya University (hp160146) and Oakforest-PACS supercomputer (hp170230, hp160146, xg18i035). The authors acknowledge valuable supports by “Priority Issue on post-K computer” (Elucidation of the Fundamental Laws and Evolution of the Universe) and “Program for Promoting Researches on the Supercomputer Fugaku” (Simulation for basic science: from fundamental laws of particles to creation of nuclei), MEXT, Japan. We also acknowledge the KAKENHI grants (17K05433, 20K03981), JSPS, Japan.

-
- [1] K. Kajino, W. Aoki, A. B. Balantekin, R. Diehl, M. A. Famiano, G. J. Mathews, *Prog. Part. Nucl. Phys.* **107**, 109 (2019).
 - [2] I. Arcavi, G. Hosseinzadeh, D. A. Howell, C. McCully, D. Poznanski, D. Kasen, J. Barnes, M. Zaltzman, S. Vasylyev, D. Maoz and S. Valenti, *Nature* **551**, 64 (2017).
 - [3] S. Shibagaki, T. Kajino, G. J. Matthews, S. Chiba, S. Nishimura, and G. Lorusso, *Astro. Phys. J.* **816**, 79 (2016).
 - [4] S. Goriely, A. Bauswein, H.-T. Janka, *Astrophys. J.* **738**, L32 (2011).
 - [5] P. A.-Soderstrom *et al.*, *AIP Conf. Proc.* **1753**, 070001 (2016).
 - [6] G. Lorusso, S. Nishimura, Z. Y. Xu *et al.*, *Phys. Rev. Lett.* **114**, 192501 (2015).
 - [7] R. Dunlop *et al.*, *Phys. Rev. C* **93**, 062801 (2016), R. Dunlop *et al.*, *Phys. Rev. C* **99**, 045805 (2019).
 - [8] H. Watanabe, G. Lorusso, S. Nishimura *et al.*, *Phys. Rev. Lett.* **111**, 152501 (2013).
 - [9] A. Jangclaus, L. Caceres, M. Gorska *et al.*, *Phys. Rev. Lett.* **99**, 132501 (2007).
 - [10] V. Manea, J. Kathrin, D. Atanasov, *et al.*, *Phys. Rev. Lett.* **124**, 092502 (2020).
 - [11] Y. Saito *et al.*, *Phys. Rev. C* **102**, 024337 (2020).
 - [12] J. Wu *et al.*, *Phys. Rev. C* **101**, 042801(R) (2020).
 - [13] H. Miyatake, M. Wada, X. Y. Watanabe, Y. Hirayama, P. Shury, M. Ahmad, H. Ishiyama, S. C. Jeong, Y. Kakiguchi, S. Kimura, J. Y. Moon, M. Mukai, M. Oyaizu, and H. Park, *AIP Conf. Proc.* **1947**, 020018 (2018).
 - [14] P. Moller, J. R. Nix, and K.-L. Kratz, *Atom. Data Nucl. Data Tab.* **66**, 131 (1997).
 - [15] P. Moller, B. Pfeiffer, and K.-L. Kratz, *Phys. Rev. C* **67**, 055802 (2003).
 - [16] J. Engel, M. Bender, J. Dobaczewski *et al.*, *Phys. Rev. C* **60**, 014302 (1999).
 - [17] I. N. Borzov, *Phys. Rev. C* **67**, 025802 (2003).
 - [18] I. N. Borzov, *Nucl. Phys. A* **777**, 645 (2006).
 - [19] H. Koura and S. Chiba, *Phys. Rev. C* **95**, 064304 (2017).
 - [20] M. T. Mustonen and J. Engel, *Phys. Rev. C* **93**, 014304 (2016).
 - [21] T. Martekin, L. Huther, and G. Martinez-Pinedo, *Phys. Rev. C* **93**, 025805 (2016).
 - [22] Z. M. Niu, H. Z. Liang, B. H. Sun, W. H. Long, and Y. F. Niu, *Phys. Rev. C* **99**, 064307 (2019).
 - [23] Q. Zhi, E. Caurier, J. J. Cuenca-Garcia, K. Langanke, G. Martinez-Pinedo, and Sieja, *Phys. Rev. C* **87**, 025803 (2013).
 - [24] J. J. Cuenca-Garcia, G. Martinez-Pinedo, K. Langanke, F. Nowacki, and I. N. Borzov, *Euro. Phys. J. A* **34**, 99-105 (2007).
 - [25] G. Marínez-Pinedo and K. Langanke, *Phys. Rev. Lett.* **83**, 4502 (1999).
 - [26] T. Suzuki, T. Yoshida, T. Kajino, and T. Otsuka, *Phys. Rev. C* **85**, 015802 (2012).
 - [27] D. H. Gloeckner and R. D. Lawson, *Phys. Lett.* **53B**, 313 (1974).
 - [28] N. Shimizu, T. Mizusaki, Y. Utsuno, and Y. Tsunoda, *Comp. Phys. Comm.* **244**, 372 (2019).
 - [29] M. Hannawald *et al.*, *Phys. Rev. C* **62**, 054301 (2020).
 - [30] J. Taprogge *et al.*, *Phys. Rev. Lett.* **112**, 132501 (2014).
 - [31] G. Audi, A. H. Wapstra, and C. Thibault, *Nucl. Phys. A* **729**, 337 (2003).
 - [32] M. Sanchez-Vega *et al.*, *Phys. Rev. C* **60**, 024303 (1999).
 - [33] B. Fogelberg and J. Blomqvist, *Phys. Lett. B* **137**, 20 (1984).
 - [34] NuDat 2.7, <http://www.nndc.bnl.gov/nudat2/>.
 - [35] M. Honma, T. Otsuka, T. Mizusaki, and M. Hjorth-Jensen, *Phys. Rev. C* **80**, 064323 (2009).
 - [36] M. Honma *et al.*, *RIKEN Accel. Prog. Rep.* **45**, 35 (2012).
 - [37] T. Otsuka, T. Suzuki, M. Honma, Y. Utsuno, N. Tsunoda, K. Tsukiyama, and M. H.-Jensen, *Phys. Rev. Lett.* **104**, 012501 (2010).
 - [38] T. Togashi, Y. Tsunoda, T. Otsuka, and N. Shimizu, *Phys. Rev. Lett.* **117**, 172502 (2016).

- [39] M. Wang, G. Audi, A. H. Wapstra *et al.*, *Chi. Phys. C* **41**, 030003 (2017).
- [40] H. Koura, T. Tachibana, M. Uno and M. Yamada, *Prog. Theor. Phys.* **113** 305 (2005).
- [41] E. Caurier, G. Martinez-Pinedo, F. Nowacki, A. Poves, and A. P. Zuker, *Rev. Mod. Phys.* **77**, 427 (2005).
- [42] R. R. Whitehead, "Moment Method in Many-Fermion Systems", p.235 (1980).
- [43] Y. Utsuno, N. Shimizu, T. Otsuka, S. Ebata, and M. Honma, *Prog. Nucl. Ener.* **82**, 102 (2015).
- [44] E. Caurier, A. Poves, and A. P. Zuker, *Phys. Rev. Lett.* **74**, 1517 (1995).
- [45] H. Watanabe *et al.*, *Phys. Lett. B* **792**, 263 (2019),
- [46] I. Dillmann *et al.*, *Phys. Rev. Lett.* **91**, 162503 (2003).
- [47] J. Liang, B. Singh, E. A. McCutchan *et al.*, *Nucl. Data Sheets* **168**, 1, (2020).
- [48] S. Yoshida, Y. Utsuno, N. Shimizu and T. Otsuka, *Phys. Rev. C* **97**, 054321 (2018).
- [49] B. Singh, J.L. Rodriguez, S.S.M. Wong, and J.K. Tuli, *Nucl. Data Sheets* **84**, 487 (1998).
- [50] B. A. Brown, *Prog. Part. Nucl. Phys.* **47**, 517 (2001).
- [51] Y. Fujita, Y. Utsuno, and H. Fujita, *Eur. Phys. J. A* **56**, 138 (2020).
- [52] M. Sasano *et al.*, *Phys. Rev. Lett.* **107**, 202501 (2011).
- [53] C. B. Hinke *et al.*, *Nature* **486**, 341 (2012).
- [54] D. Lubos *et al.*, *Phys. Rev. Lett.* **122**, 222502 (2019).
- [55] K. L. G. Heyde, *The Nuclear Shell Model* (Springer-Verlag, Berlin, 1994), 2nd ed., Sec. 3.4.3.